Int. J. Nanosci. Nanotechnol., Vol. 19, No. 2, June 2023, pp. 121-134
DOI: 10.22034/ijnn.2023.2001625.2372

Effects of Graphene Oxide Size on PES Ultrafiltration Hydrophilicity and Pure Water Flux

Zahra Madanirad[1], Mahdi Akbari[1], Mojtaba Shariaty-Niassar[1,*] and Karim Akbari Vakil Abadi[2]

[1]Transport Phenomena & Nanotech. Lab (TPNT), School of Chemical Engineering, College of Engineering, University of Tehran, P.O. Box: 11155-4563, Tehran, Iran
[2]Department of Mechanical Engineering, Imam Khomeini Naval University, Noshahr, Iran

(*) Corresponding author: mshariat@ut.ac.ir
(Received: 30 April 2023 and Accepted: 21 May 2023)

Abstract

In this study, the effects of graphene oxide (GO) size on the structure and performance of polyethersulfone/graphene oxide nanocomposite ultrafiltration membrane (prepared via phase inversion method) were studied. Graphene oxide was synthesized by Hummers method and was divided into two parts with different sizes (80 nm and 110 nm) by means of centrifugation (10000 rpm). Synthesized GO was characterized by FESEM, TEM, Raman spectroscopy, FTIR, XRD and DLS. Prepared membranes were characterized by FESEM, AFM, contact angle and pure water permeation flux. Interestingly, decrease in PWP permeance was observed with an increase in the concentration of smaller GO in the membrane, while the trend was reversed by the addition of the larger GO. As a result, the maximum PWP permeance of 21 kg/m^2 h bar was achieved when the smaller GO concentration was 0.1 wt.% while 23 kg/m^2 h bar was achieved when the larger GO concentration was 1 wt.%. This opposite trend is ascribed to the readiness of smaller GO nanosheets to aggregate. The antifouling capacity of nanocomposite membranes was found to be higher than the pristine PES membrane.

Keywords: *Graphene oxide, Polyethersulfone, Membrane, Phase inversion, Anti-fouling properties.*

1. INRODUCTION

Today, global concerns about the lack of freshwater resources in the world are increasing and seawater desalination is considered as an important approach for solving this crisis. Many efforts have been made to produce potable water from seawater, e.g. membrane filtration, electro-dialysis, distillation, ion exchange, and freezing. Among those, reverse osmosis (RO) is one of the most attractive for many researchers, because of their simplicity, easy scale up, continuous operation, low space requirement, and low cost due to the absence of phase change [1]. But RO also suffers from serious fouling problem due to the presence of colloidal substances, suspended solids, dissolved organic matter and minerals in feed water [2]. Hence it is imperative to remove these foulants by pretreatment before the feed stream enters into the RO module. Ultrafiltration is nowadays gaining popularity as the seawater pretreatment because of the advantages such as selective separation, automatic and continuous operation, easy scaling, low space requirements and low energy costs in particular. But the pore size of ultrafiltration membrane is in the range of many macromolecules. Because of this reason, fouling caused by the adsorption of particles into the pores of ultrafiltration membrane is one of the most challenging problems for this method [3].

To fabricate ultrafiltration membranes, polymeric materials such as polysulfone [4], polyethersulfone [5], polyamide [6] and polyvinylidene fluoride [7] are often used. Among those, PES is one of the most widely used polymers due to its high thermal stability, resistance to chemicals,

good mechanical strength, good solubility in some aprotic solvent and so on. PES is also used to prepare membranes for nanofiltration, microfiltration, and reverse osmosis. But low hydrophilicity of this polymer is the cause of low flux and low antifouling capacity in practical applications. Many efforts have been made to improve their hydrophilicity and filtration performance, such as adding hydrophilic polymers [8, 9], or hydrophilic nanoparticles [10-16] and membrane surface modification [17, 18].

Graphene oxide (GO) is a nanomaterial that has been frequently blended in polymeric membranes due to its excellent properties such as high specific surface area and hydrophilicity [19-22]. It has been shown that GO has a high and adjustable hydrophilicity. But strangely enough, the optimum concentration of GO in the membranes varies from researcher to researcher. Hu et al .[23] investigated the effect of GO size on its hydrophilicity and showed that the hydrophilicity of GO depends on its size since GO's ionizable groups are affected by the size. This man be the reason for the variety of the optimum GO concentration reported in the literature. Shen et al. [24] also examined the effect of GO nanosheets size on the performance of membranes for the removal of carbon dioxide.

In this research, we investigated the effect of GO size on the properties of PES ultrafiltration membranes. GO was prepared by Hummers method and separated into two fractions of different sizes. Each fraction was used in three different concentrations (0.1-0.5 and 1) in the casting dope to fabricate nanocomposite membranes and characterization and performance evaluation of the membranes were carried out.

2. MATERIALS

N-methyl-2-pyrrolidone (NMP) (Mw= 99.13 g/mol and d=1.03 g/cm3), sulfuric acid (H_2SO_4, 95-97 wt. %), nitric acid (HNO_3, 56 wt. %), hydrogen peroxide (H_2O_2), hydrochloric acid (HCl, 37 wt. %), sodium hydroxide (NaOH) and potassium permanganate ($KMnO_4$) were supplied from Merck. Polyethersulfone (PES) (Ultrason E 6020P, Mw=58,000 g/mol and glass transition temperature Tg=220˚C) was obtained from BASF. Bovine serum albumin (BSA) (Mw=68,000 g/mol) and flake graphite were purchased from Sigma Aldrich. Phosphate buffer was supplied by an Iranian company (Vaheb). Deionized water was used in all of experiments.

3. METHODS

3.1. GO Synthesis

GO was synthesized by Hummers method. 225 mL of sulfuric acid was mixed with 85 mL of nitric acid at 1˚C in a Two-chamber reactor connected to a circulator. When the temperature of solution became near 3˚C, 7 g of graphite powder was added. The suspension was stirred for 1 h, before 42 g of potassium permanganate was slowly added to solution during a 2 h period. Then, the temperature was raised to 36 ˚C and the mixture was stirred with a mechanical stirrer (650 rpm) for 2 days, followed by the increase of temperature to 97 ˚C and stirring (900 rpm) for 15 min. The temperature was then decreased to 30˚C and 70 ml of H_2O_2 was added slowly. The suspension was left for 24 h to let the product GO precipitate to the bottom, which was followed by the removal of top water layer. The bottom residue was first washed with HCl (2 wt. %) for the removal of metal ions and then several time with distilled water until pH became neutral. Graphite oxide so prepared was dispersed in distilled water by sonication for 3 h and centrifuged at 1500 rpm for ensuring that remaining graphite was removed. The supernatant was further divided to two parts (on the basis of size) by centrifugation at 10000 rpm for 40 min. Finally, both parts were filtered and dried at 50˚ for 48 hours.

3.2. Preparation of GO/PES Mixed Matrix Membrane

GO/PES mixed matrix membranes were fabricated by the phase inversion method. Seven membranes with different composition were prepared (Table 1). The casting dope contained PES (15%wt), NMP and GO of different sizes and concentrations (0.1, 0.5, 1 wt. % relative to PES) as additives. First, GO was dispersed in NMP by sonication for 2 h, followed by stirring with magnetic stirrer for 20 min. Then, PES was added under continuous stirring (100 rpm) for 20 h to make uniform casting dope, which was then left for 5 h to remove air bubbles prior to casting onto a clean glass plate using a casting knife. After 30 s, the cast film together with the glass plate was immersed into a distilled water bath at temperature 25±0.5 °C. After 20 min the membrane, which peeled off from the glass plate spontaneously, was transferred to fresh distilled water and kept there for 24 h to complete the phase separation. Finally membranes were dried at room temperature for 24 h.

***Table 1**. Composition of casting solutions*

No.	Membrane Code	Additive		PES (wt. %)
		Small GO (wt. %)*	Large GO (wt. %)*	
1	PES	-	-	15
2	SGO-0.1	0.1	-	15
3	SGO-0.5	0.5	-	15
4	SGO-1	1	-	15
5	LGO-0.1	-	0.1	15
6	LGO -0.5	-	0.5	15
7	LGO -1	-	1	15

*Additives wt. % is based on the PES.

3.3. Characterization of GO

Functional groups of graphene oxide (hydroxyl, carbonyl, ether, and carboxyl) were identified using Fourier Transform Infrared Spectroscopy (FT-IR, PerkinElmer). For FT-IR analysis, the GO samples were pressed into KBr pellets. For structural characterization of GO, Raman spectroscopy (Teksan model Takram P50C0R10) with an excitation laser at 532 nm and a range of 200-2000 cm^{-1} was used. X-Ray diffraction (XRD) patterns were observed by Siemens X-ray Powder Diffraction Diffractometer D5000 with Cu Kα radiation. The morphology of graphene oxide was investigated using field emission scanning electron microscope (FE-SEM, ZEISS VP). For sample preparation, GO was dispersed in ethanol by probe sonication and then a drop was deposited on lamella and was dried at 50 °C. Further observation of GO was performed by transmission electron microscopy (TEM, Philips CM30 electron microscope). In order to determine size distribution of GO nanosheets, Dynamic Light Scattering (DLS) analysis was carried out by ZEN3600 Molvern zetasizer. For this purpose, 1 mg/mL suspension of both sizes of GO in NMP was made by sonication (for 30 min).

3.4. Characterization of Membranes

Structure and cross-sectional morphology of membranes were observed by a scanning electron microscope (SEM, Zeiss DSM-960A). Samples (wet) were fractured in liquid nitrogen and then sputter-coated with gold to enhance their conductivity. Surface morphology of PES, SGO-0.1 and LGO-1 membranes was observed by AFM (NTEGRA AURA NTMDT, Russia, semi-contact mode) at room temperature in air. The average (R_a) and root-mean-square (R_{rms}) roughness for three images of each membrane were determined and the average values were reported. Contac angle measurements were carried out

based on sessile-drop method. For each measurement, 5 μL deionized water droplet was placed by a Hamilton syringe on the membrane surface and immediately a picture was taken by digital microscope. Then ImageJ software was used to determine contact angle. The measurement was made at five random spots of each membrane and the average value was reported.

3.5. Performance Evaluation of Membranes

The performance of the membranes was evaluated by the pure water permeation (PWP) and ultrafiltration tests using BSA feed solution. The tests were carried out with a self-made dead-end stirred filtration setup (effective area, 13 cm^2). First, the membrane was compacted at 0.6 MPa for 30 min to achieve a steady flux, followed by a PWP test at 0.2 MPa. PWP (Jw_1, kg/m^2 h) was calculated every 5 min by the following equation:

$$J_{w1} = \frac{M}{A\Delta t} \quad (1)$$

where M is the weight of permeate collected (kg) during time Δt (h), and A is the membrane effective area (m^2). All experiments were carried out at ambient temperature. The permeance (kg/m^2 h bar) is defined as the flux normalized by the transmembrane pressure difference.

After 1 h of PWP test the distilled water was switched to 0.2 mg/mL BSA solution and the UF test was continued for another 1 h. The flux was calculated every 5 min by the equation (1), where J_p is used instead of J_{w1}. After 1 h, fouled membrane was taken away from setup and its surface was washed with some distilled water. Then for better cleaning, it was put into distilled water for 40 min. During this period, fresh distilled water was replaced every 10 min. Then the PWP of cleaned membrane (J_{w2}) was measured every 5 min by the equation (1). The flux recovery ratio (FRR) was calculated by the following equation:

$$FRR = \frac{J_{w2}}{J_{w1}} \times 100\% \quad (2)$$

4. RESULT AND DISCUSSION

4.1. Characterization of GO Nanosheets

4.1.1. FTIR Analysis of GO Nanosheets

FTIR spectra of GO nanosheets are shown in Figure 1. The result is consistent with the those of the FTIR analysis reported in the literature [25, 26]. The peaks at 3413 and 1383 cm^{-1} relate to the stretching and deformation vibration of the O-H, respectively. The peak at 1731 cm^{-1} represents a stretching vibration of C = O band, and peaks at 1051 and 1186 cm^{-1} result from the stretching vibration of C-O in that indicates the formation of carboxylic acid on the edges and surface of graphene oxide. A peak at 1626 cm^{-1} indicates the vibration of absorbed water molecules or the epoxide group (ring ether) [27]. Thus, all the functional groups of graphene oxide are observed in the synthesized sample.

4.1.2. Raman Spectroscopy

Raman spectrum of GO nanosheets is presented in Figure 2. Two main GO peaks can be observed located at ~1350 and ~1590 cm^{-1} for the D and G bands, respectively that are in agreement with literature [28, 29].

4.1.3. FESEM and TEM Observation

FESEM and TEM images of GO nanosheets are exhibited in Figure 3. Obviously, layered and folded structure of GO nanosheets with wrinkled surface can be seen. After oxidation, morphology of graphite plates significantly altered and gap between the sheets was increased and its surface and edges became wrinkled [30].

4.1.4. XRD Analysis

XRD patterns of graphene oxide is presented in Figure 4. Characteristic peak of graphene oxide at 2θ~8˚ is in accordance with the reported values in the literature [31, 32]. The lack of peaks at

2θ~23˚ and 2θ~26˚, indicates absence of graphite and reduced graphene oxide, respectively [32-34].

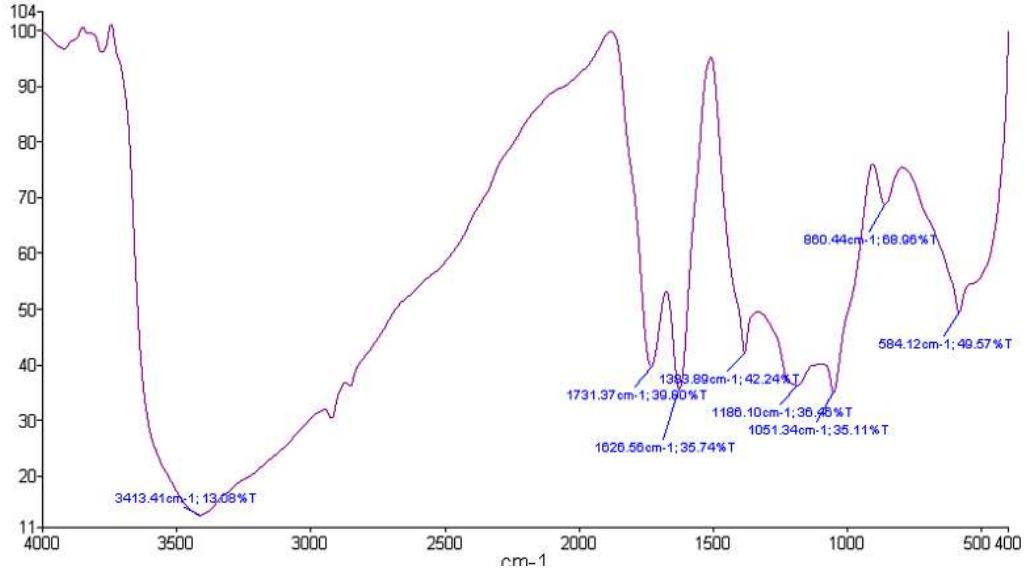

Figure 1*. The FTIR spectrum of synthesized graphene oxide.*

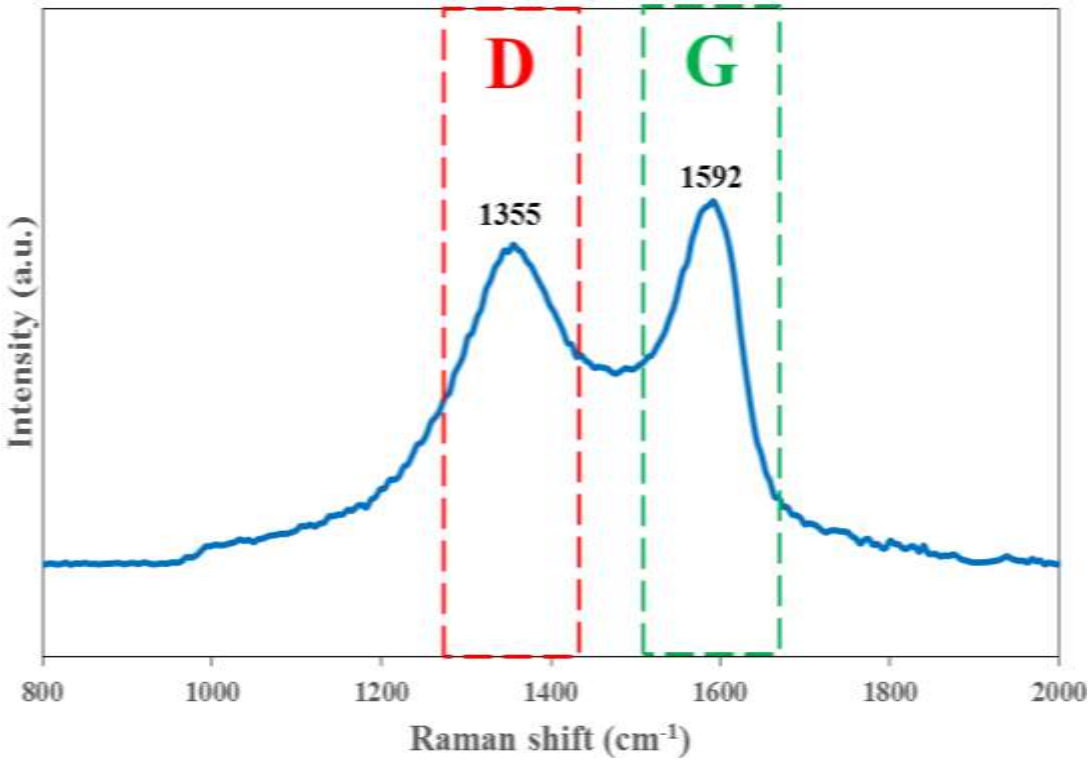

Figure 2. *Raman spectroscopy of synthesized GO nanosheets.*

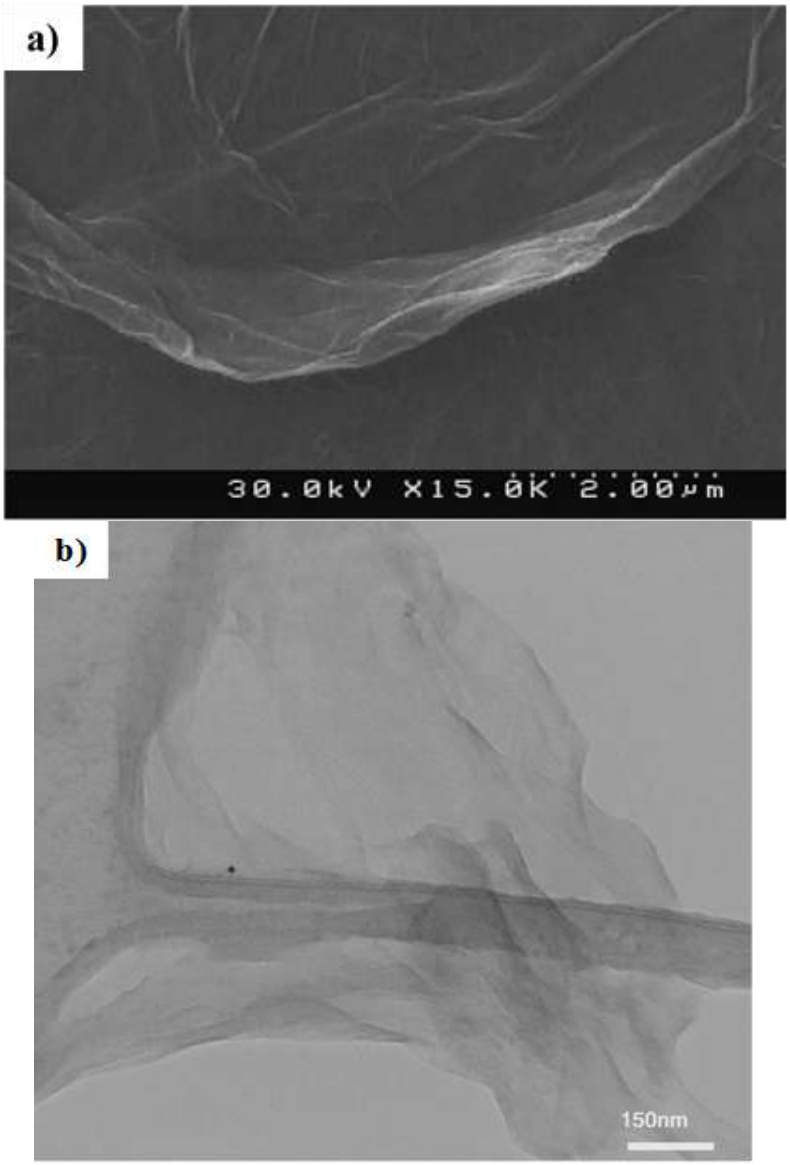

Figure 3. *GO nanosheets a) FESEM and b) TEM images.*

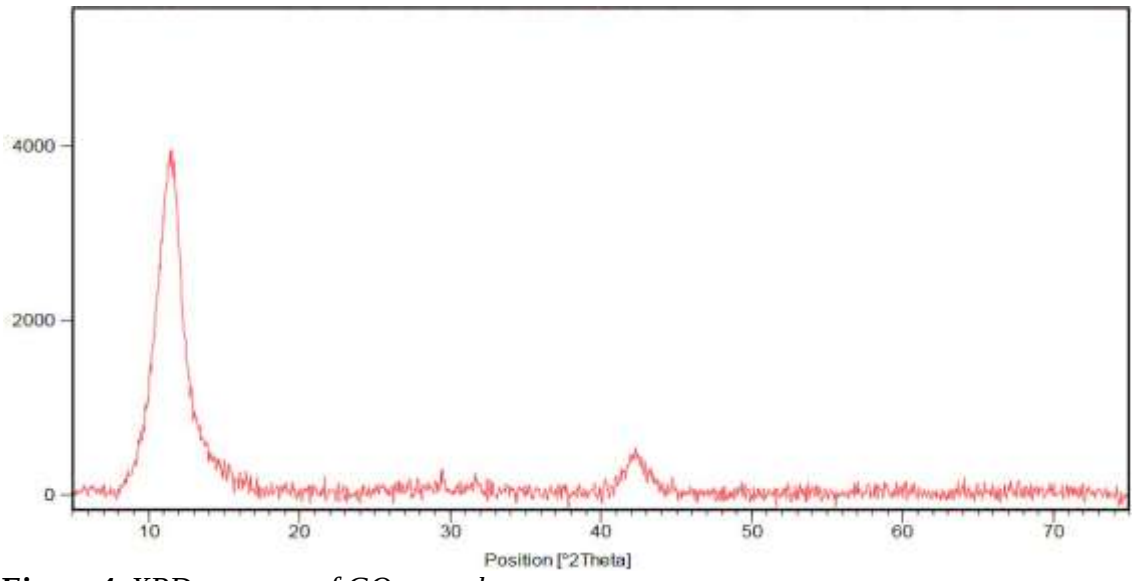

Figure 4. *XRD patterns of GO nanosheets.*

4.1.5. Size Distribution of GO Nanosheets

Figure (5a) and (5b) show the DLS analysis of SGO and LGO nanosheets, respectively. SGO has a sharp peak at 91.8 nm and a weak peak at 1050 nm. LGO has two peaks at 151 and 740 nm. These results show the size difference between SGO and LGO nanosheets.

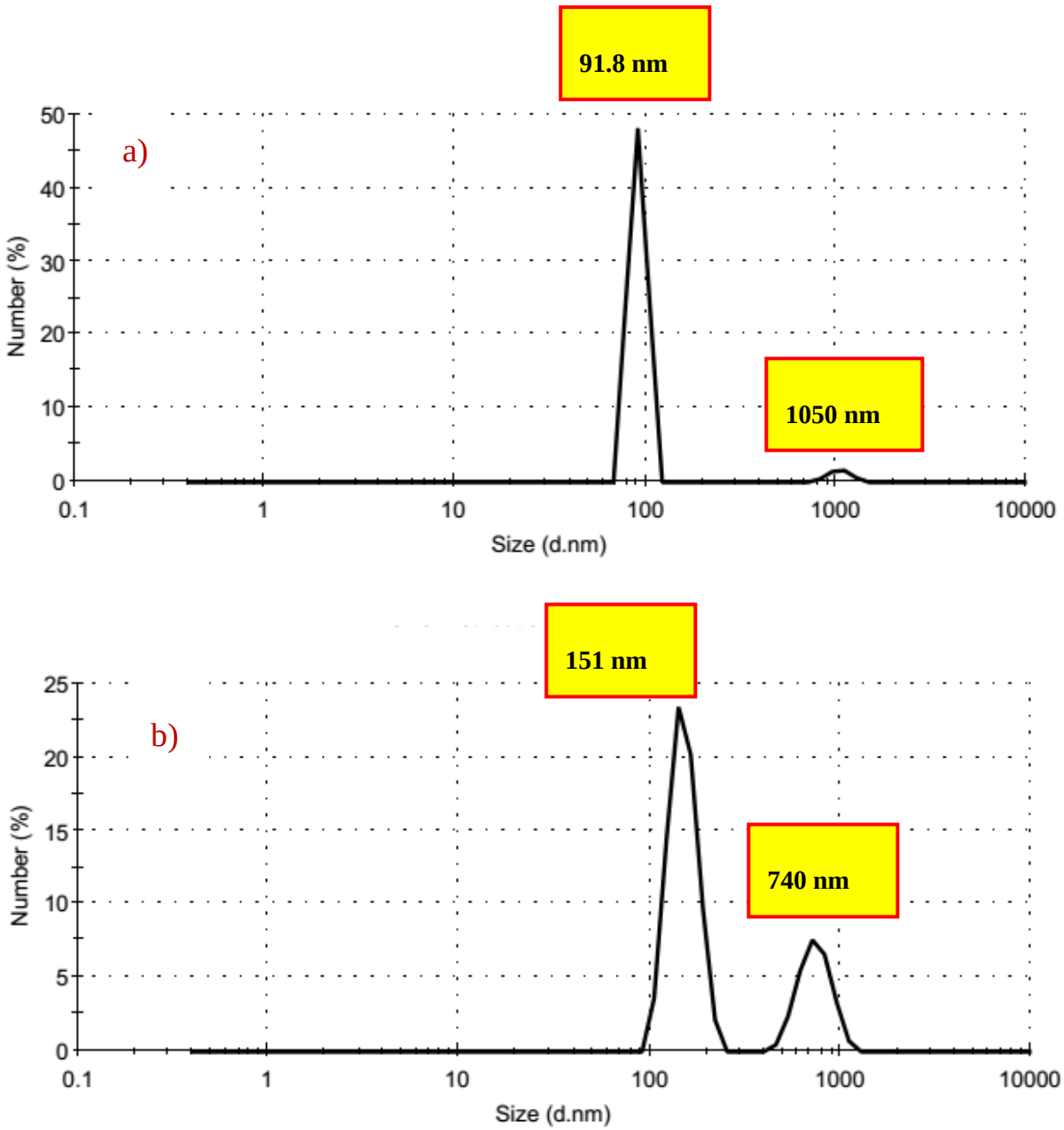

Figure 5. *Size distribution of a) SGO and b) LGO.*

4.2. Characterization of Prepared Membranes

4.2.1. SEM Analysis

SEM cross-sectional images of the prepared membranes are shown in Figures 6 and 7. As it can be seen, membranes have asymmetric structure with a thin selective layer and finger-like macrovoids in the sub-layer. Adding hydrophilic GO in casting solution increases thermodynamic instability and speeds up the nonsolvent (water) intrusion into the cast film during the solvent/nosnsolvent exchange process, which results in thinner selective layer and larger finger-like pores in the substrate [30].

GO nanosheets also act as a connection point between polymer chains, creating a structure with higher pore density [35]. As it is clear in Figure 6, the number of channels just below the top skin layer increases upon adding GO in agreement with other preceding studies. The largest number of channels is found at 0.1% and 1%, respectively, for SGO and LGO. Thus, GO controls the amount and distribution of finger-like channels [24].

GO size has a great impact on the structure and properties of mixed matrix membranes. This parameter can be set polymer chains moving so that by increasing the size of nanosheets, polymers tend to find solid stems. In general, due to the interactions of graphene oxide nanosheets and polyether sulfone with high hydrogen networks forming, the polymer chins moving is limited and this limiting increase with increase size of graphene oxide. Polymer chains are discrete when larger fillers placed in polymer matrix [24].

For smaller GO, number of pores with less width increase, that also coordinate water flux values pass through the membrane.

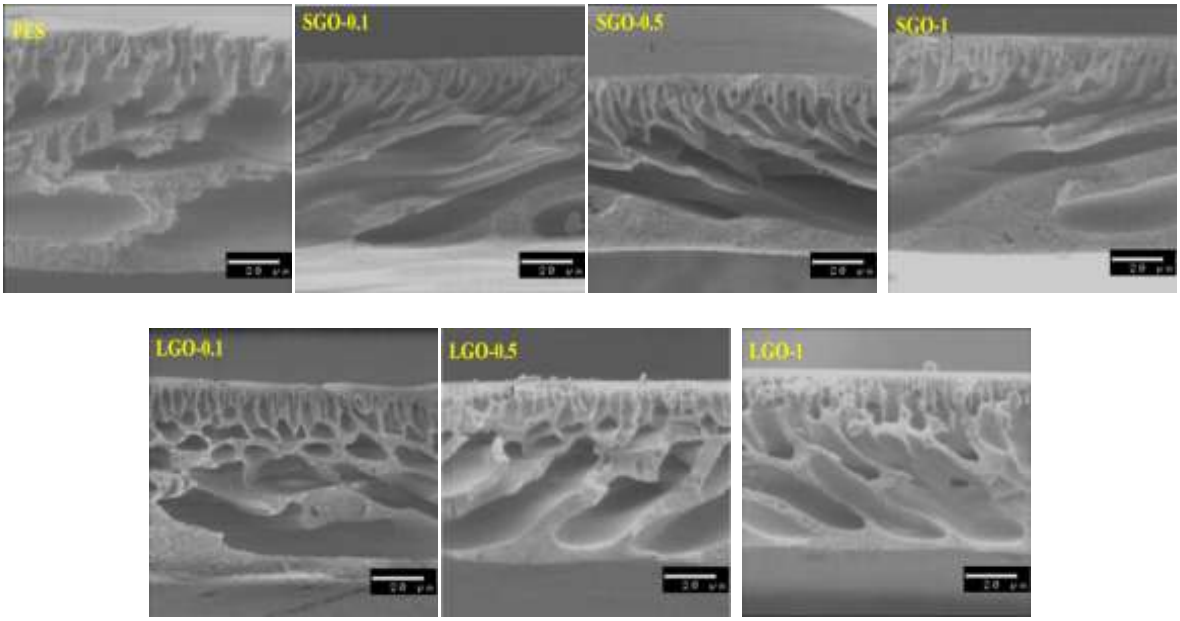

Figure 7. *SEM cross-sectional images of the prepared membranes.*

4.2.2. Contact Angle Measurement

The results of the contact angle measurement are summarized in Figure 8. From the figure the change in contact angle is only marginal. But the following trends are observed, i.e. upon addition of SGO contact angle decreases but further addition of SGO tends to increase the contact angle. The initial decrease in contact angle (increase in hydrophilicity) seems to be due to the presence of hydrophilic functional groups on GO surface. The increase in contact angle seems to be due to the aggregation of SGO nanoparticles.

In case of LGO. The contact angle keeps decreasing with the amount of LGO addition. This indicates the lesser trend of aggregation when the GO size is larger.
Another interpretation is leaching out of SGO nanoparticles from the casting dope to nonsolvent water, which reduces the hydrophilicity of the membrane. Less leaching occurs when the GO size is as large as that of LGO.

4.2.3. Pure Water Permeation Flux

Figure 9 shows PWP permeance of the prepared membranes. It is found that adding GO into the membrane, increases PWP flux regardless of the size and

amount of the added GO nanosheets. This is due to the thinning of the top skin layer and increase in the finger-like pore density by the addition of GO nanosheets, as observed in SEM images shown in Figures 6 and 7.

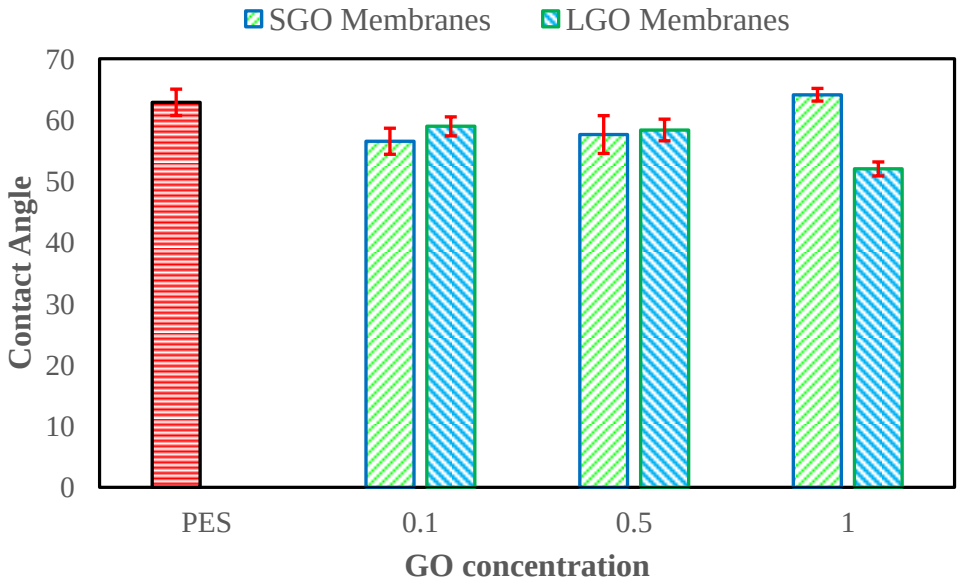

Figure 8. *Contact angle of synthesized membranes.*

As for the effect of GO nanosheets concentration, it is interesting to note that the trend observed in PWP permeance is closely correlated to the contact angle change, i.e. with an increase in SGO concentration contact angle increases, while PWP permeance decreases. On the other hand, with an increase LGO concentration, the contact angle decreases while the PWP permeance increases. It can therefore be concluded that decrease in the membrane contact angle (increase in surface hydrophilicity) enhances the PWP permeance.

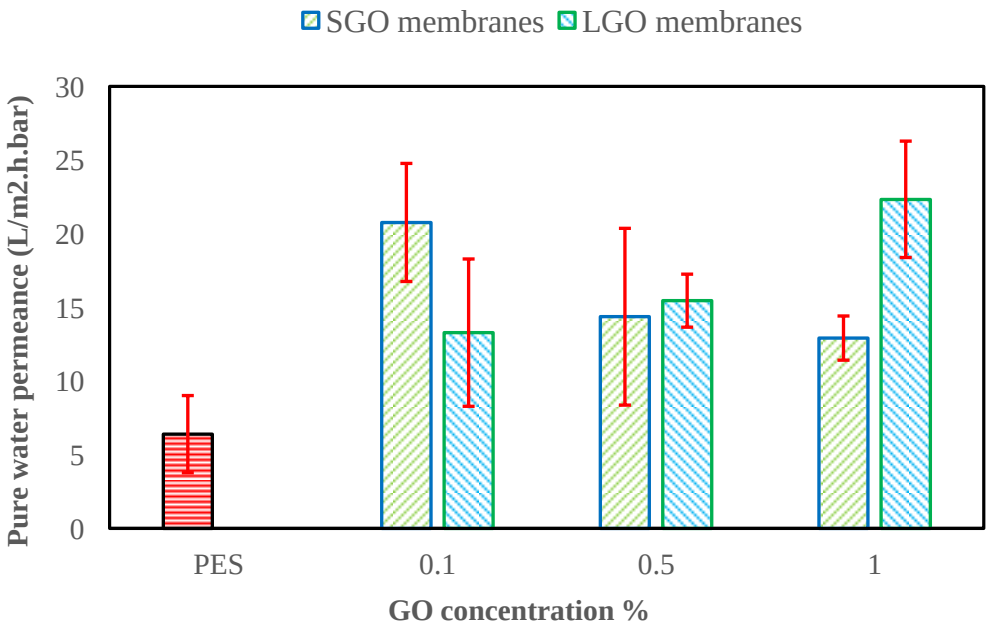

Figure 9. *Pure water permeance vs GO concentration.*

From Figure 9, the maximum PWP permeance of 21 kg/m^2 h bar was obtained at 0.1wt.% SGO concentration, while 23 kg/m^2 h bar was obtained at 1 wt.% LGO concentration. Hence these two membranes, together with the pristine PES membrane were used for the fouling study.

4.2.4. Stability of GO

To evaluate the aggregation tendency of GO, DLS analysis was carried out for both SGO and LGO. SGO and LGO were dispersed in NMP and after 1 h of sonication the particle size was measured by DLS. Figure 10 shows the DLS results. It could be observed that the size of SGO enhanced from 91.8 nm to 114 nm (24.2%) but the size of LGO enhanced from 151 nm to 179 nm (18.5%), confirming that GO nanosheets trend to aggregate more than LGO nanosheets.

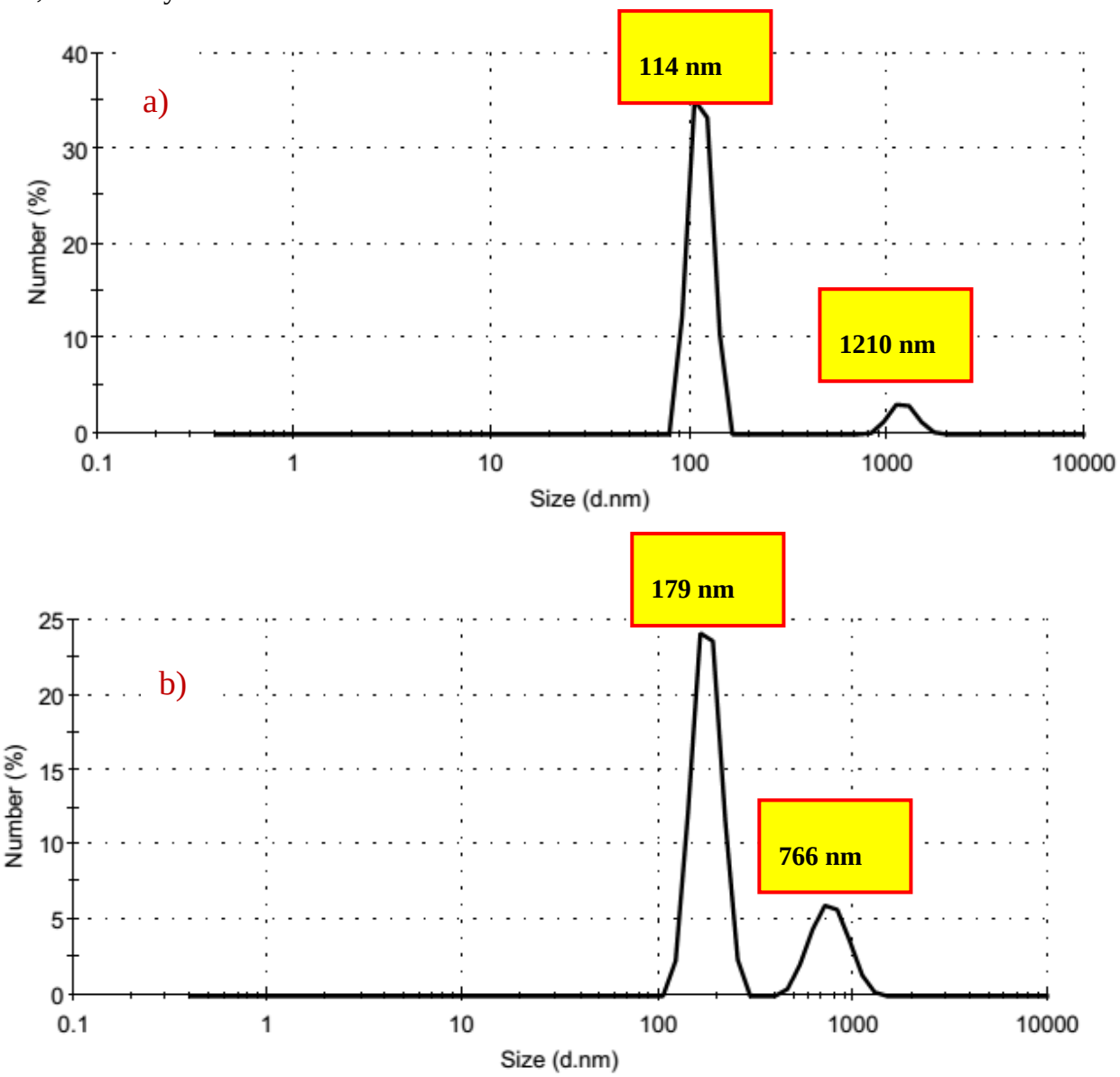

Figure 10. *Size distribution of a) SGO and b) LGO.*

4.2.5. Anti-Fouling Analysis

Fig. 12 shows the permeate flux of the PES, SGO-0.1 and LGO-1 membranes before, during and after BSA filtration. It is interesting to note that significantly higher fluxes of SGO-0.1 and LGO-1 than PES are retained during and after the BSA tests. Flux recovery ratio (FRR) was calculated by equation (2) and the results shown in Figure 13. From the figure FRR

of PES, SGO-0.1 and LGO-1 is 32, 46.88 and 41.49 %, respectively, indicating the better fouling resistance of SGO-0.1 and LGO-1 than pristine PES. Between SGO-0.1 and LGO-1, SGO-1 is higher. This result cannot be ascribed to the rather marginal difference between the contact angles. Hence, the surface roughness, which is another parameter to affect the fouling, was measured by AFM.

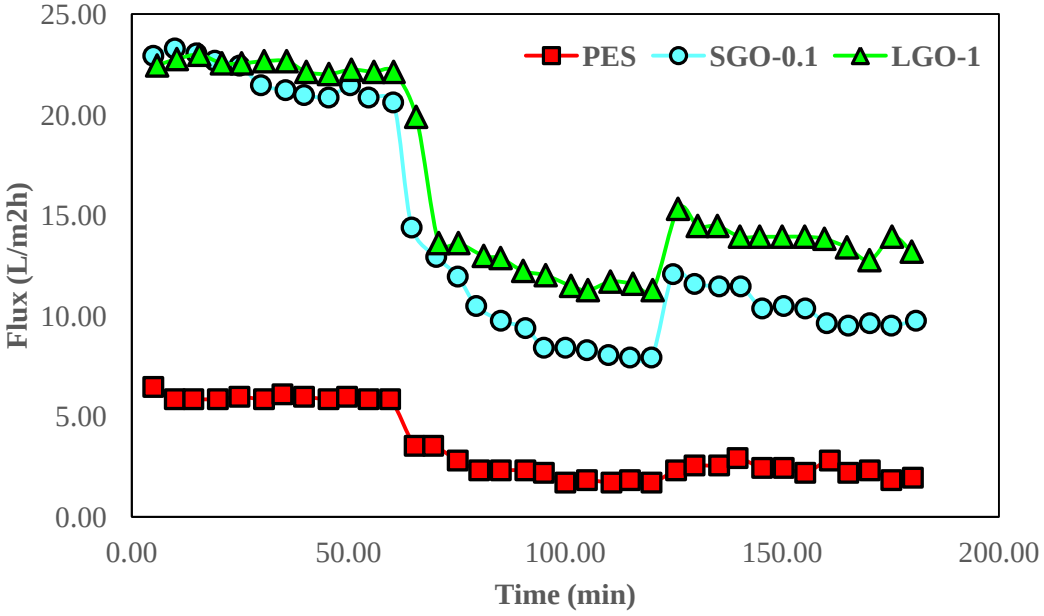

Figure 12. *Flux versus time for the PES, SGO-0.1 and LGO-1 membranes during three steps for fouling test.*

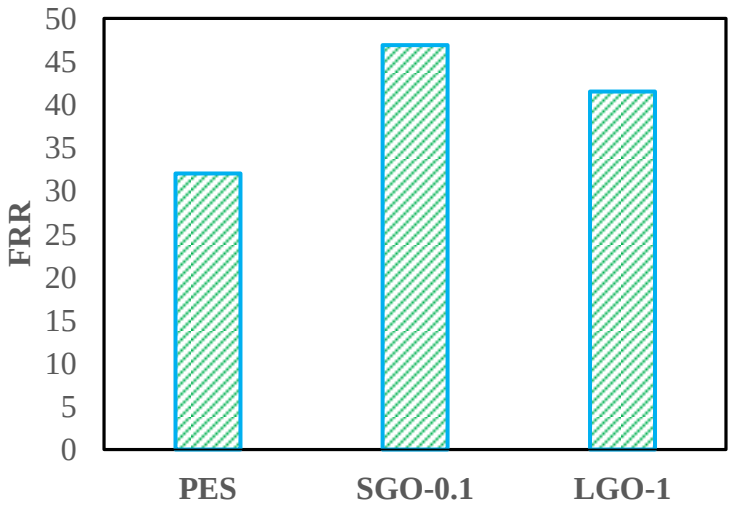

Figure 13. *FRR value for synthesized membranes with different size of GO.*

4.2.6. AFM

Figure 14 shows 2-D and 3-D AFM images of PES, SGO-0.1 and LGO-1 membranes surface. Two roughness parameters of the membranes (R_a and R_{rms}) were obtained by the built-in software and the results shown in Table 3. From Fig. 14 PES pristine membrane has a typical ridgevalley morphology. For SGO-0.1 the depth of the valley diminished. For LGO-1 size and intensity of the bright spots increased. Correspondingly, the surface roughness parameter decreased from PES to SGO-0, 1 and then increased from SGO-0.1 to LGO-1 (Table 3). The smoother surface of SGO-0.1 than LGO-1 is hence likely the reason for the higher antifouling capacity of SGO-0.1 than LGO-1.

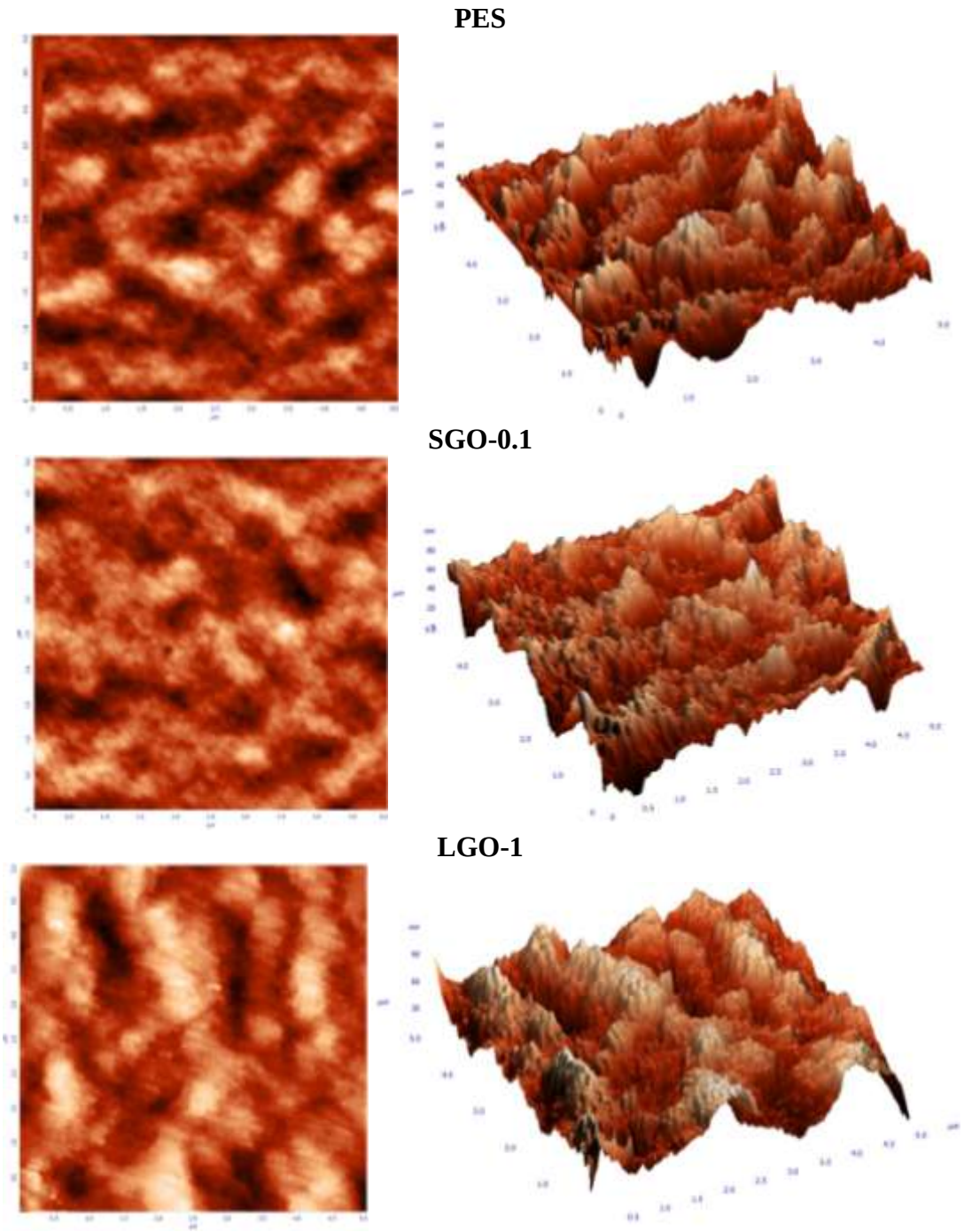

Figure 14. *AFM images of PES, SGO-0.1 and LGO-1 membranes surface.*

Table 3*.Roughness parameters of PES, SGO-0.1 and LGO-1 membranes.*

Sample	R_a	R_{rms}
PES	10.26±0.204	12.765±0.219
SGO-0.1	9.214±0.173	11.664±0.194
LGO-1	10.573±1.09	13.438±1.347

5. CONCLUSION

In this study the effect of the size of GO and its concentration in the GO/PES nanocomposite membrane on the membrane properties and performance was investigated. There are two different effects of GO nanosheets concentration, i.e. for smaller GO the contact angle

increases and the PWP permeance decreases as the GO concentration increases, while the trend is opposite for the larger GO. This is attributed to the readiness of smaller GO nanosheets, as evidenced by an independent experiment on GO aggregation in NMP. As a result, the maximum PWP permeance of 21 kg/m^2 h bar at the SGO concentration of 0.1 % and 23 kg/m^2 h bar at LGO concentration of 1 % were achieved. As for the fouling test, SGO-0.1 showed the highest antifouling capacity among pristine PES, SGO-1 due to its high hydrophilicity and smoothness of the membrane surface.

Acknowledgement

The authors are thankful to Iran National Science Foundation (INSF) for funding this research under contract number 92013505.

CONFLICT OF INTEREST

The authors declare that they have no conflict of interest.

REFERENCES

1. Sahinkaya, E., "Concentrate minimization and water recovery enhancement using pellet precipitator in a reverse osmosis process treating textile wastewater",. *Journal of Environmental Management*, 222 (2018) 420-427.
2. Jiang, S., Y. Li, Ladewig, B. P. "A review of reverse osmosis membrane fouling and control strategies", *Science of The Total Environment*, 595 (2017) 567-583.
3. Shi, X., "Fouling and cleaning of ultrafiltration membranes: A review*", Journal of Water Process Engineering*, 1 (2014) 121-138.
4. Yang, Y., "The influence of nano-sized TiO2 fillers on the morphologies and properties of PSF UF membrane", *Journal of Membrane Science*, 288(1-2) (2007) 231-238.
5. Zinadini, S., "Preparation and characterization of antifouling graphene oxide/polyethersulfone ultrafiltration membrane: Application in MBR for dairy wastewater treatment", *Journal of Water Process Engineering*, 7 (2015) 280-294.
6. Rakhshan, N., Pakizeh, M., "The effect of chemical modification of SiO2 nanoparticles on the nanofiltration characteristics of polyamide membrane", *Korean Journal of Chemical Engineering*, 32(12) (2015) 2524-2533.
7. Wang, Q., "Impact of sodium hypochlorite cleaning on the surface properties and performance of PVDF membranes", *Applied Surface Science*, 428 (2018) 289-295.
8. Rahimpour, A., Madaeni, S., "Polyethersulfone (PES)/cellulose acetate phthalate (CAP) blend ultrafiltration membranes: preparation, morphology, performance and antifouling properties", *Journal of Membrane Science*, 305(1) (2007) 299-312.
9. Qu, P., "Polyethersulfone composite membrane blended with cellulose fibrils", *BioResources*, 5(4) (2010) 2323-2336.
10. Vatanpour, V., "TiO2 embedded mixed matrix PES nanocomposite membranes: influence of different sizes and types of nanoparticles on antifouling and performance", *Desalination*, 292 (2012) 19-29.
11. Jin, F., "High-performance ultrafiltration membranes based on polyethersulfone–graphene oxide composites", *Rsc Advances*, 3(44) (2013) 21394-21397.
12. Van der Bruggen, B., "Chemical modification of polyethersulfone nanofiltration membranes: a review", *Journal of applied polymer science*, 114(1) (2009) 630-642.
13. Liu, Y., "Improved antifouling properties of polyethersulfone membrane by blending the amphiphilic surface modifier with crosslinked hydrophobic segments", *Journal of Membrane Science*, 486 (2015) 195-206.
14. Moghimifar, V., "Enhancing the antifouling property of polyethersulfone ultrafiltration membranes using NaX zeolite and titanium oxide nanoparticles", *RSC Advances*, 5(69) (2015) 55964-55976.
15. Amirilargani, M., Saljoughi, E., Mohammadi, T., "Effects of Tween 80 concentration as a surfactant additive on morphology and permeability of flat sheet polyethersulfone (PES) membranes", *Desalination*, 249(2) (2009) 837-842.
16. Farahani, M. H. D. A., Rabiee, H., Vatanpour, V., "Comparing the effect of incorporation of various nanoparticulate on the performance and antifouling properties of polyethersulfone nanocomposite membranes", *Journal of Water Process Engineering*, 27 (2019) 47-57.
17. Rahimpour, A., "UV photo-grafting of hydrophilic monomers onto the surface of nano-porous PES membranes for improving surface properties", *Desalination*, 265(1) (2011) 93-101.
18. Shi, Q., "Grafting short-chain amino acids onto membrane surfaces to resist protein fouling", *Journal of Membrane Science*, 366(1) (2011) 398-404.

19. Dave, H. K., Nath, K., "Graphene oxide incorporated novel polyvinyl alcohol composite membrane for pervaporative recovery of acetic acid from vinegar wastewater", *Journal of Water Process Engineering*, 14 (2016) 124-134.
20. Song, N., "A review of graphene-based separation membrane: Materials, characteristics, preparation and applications", *Desalination*, 437 (2018) 59-72.
21. Abdel-Karim, A., "High flux and fouling resistant flat sheet polyethersulfone membranes incorporated with graphene oxide for ultrafiltration applications", *Chemical Engineering Journal*, 334 (2018) 789-799.
22. Zhu, Z., "Preparation and characteristics of graphene oxide-blending PVDF nanohybrid membranes and their applications for hazardous dye adsorption and rejection", *Journal of colloid and interface science*, 504 (2017) 429-439.
23. Hu, X., "Effects of particle size and pH value on the hydrophilicity of graphene oxide", *Applied Surface Science*, 273 (2013) 118-121.
24. Shen, J., "Size effects of graphene oxide on mixed matrix membranes for CO2 separation", *AIChE Journal*, (2016).
25. Wang, G., "Synthesis of enhanced hydrophilic and hydrophobic graphene oxide nanosheets by a solvothermal method", *Carbon*, 47(1) (2009) 68-72.
26. Sun, H., Cao, L., Lu, L., "Magnetite/reduced graphene oxide nanocomposites: one step solvothermal synthesis and use as a novel platform for removal of dye pollutants", *Nano Research*, 4(6) (2011) 550-562.
27. Zinadini, S., "Preparation of a novel antifouling mixed matrix PES membrane by embedding graphene oxide nanoplates", *Journal of Membrane Science*, 453 (2014) 292-301.
28. Li, P., "Synthesis, characterization, and bactericidal evaluation of chitosan/guanidine functionalized graphene oxide composites", *Molecules*, 22(1) (2016) 12.
29. Rana, S., Maddila, S., Jonnalagadda, S. B., "Synthesis and characterization of Pd (II) dispersed over diamine functionalized graphene oxide and its scope as a catalyst for selective oxidation", *Catalysis Science & Technology*, 5(6) (2015) 3235-3241.
30. Ganesh, B., Isloor, A. M., Ismail, A., "Enhanced hydrophilicity and salt rejection study of graphene oxide-polysulfone mixed matrix membrane", *Desalination*, 313 (2013) 199-207.
31. Marcano, D. C., "Improved synthesis of graphene oxide", *ACS Nano*, 4(8) (2010) 4806-4814.
32. Zhang, L., "Size-controlled synthesis of graphene oxide sheets on a large scale using chemical exfoliation", *Carbon*, 47(14) (2009) 3365-3368.
33. Shin, H. J., "Efficient reduction of graphite oxide by sodium borohydride and its effect on electrical conductance", *Advanced Functional Materials*, 19(12) (2009) 1987-1992.
34. Park, S., "Hydrazine-reduction of graphite-and graphene oxide", *Carbon*, 49(9) (2011) 3019-3023.
35. Zhao, Y., "Performance enhancement of polyvinyl chloride ultrafiltration membrane modified with graphene oxide", *Journal of Colloid and Interface Science*, 480 (2016) 1-8.